




# Catching a Planet: A Tidal Capture Origin for the Exomoon Candidate *Kepler 1625b I*

Adrian S. Hamers<sup>1</sup>  and Simon F. Portegies Zwart<sup>2</sup><sup>1</sup> Institute for Advanced Study, School of Natural Sciences, Einstein Drive, Princeton, NJ 08540, USA; [hamers@ias.edu](mailto:hamers@ias.edu)<sup>2</sup> Leiden Observatory, Leiden University, P.O. Box 9513, NL-2300 RA Leiden, The Netherlands; [spz@strw.leidenuniv.nl](mailto:spz@strw.leidenuniv.nl)

Received 2018 October 25; revised 2018 November 21; accepted 2018 November 23; published 2018 December 14

## Abstract

The (yet-to-be confirmed) discovery of a Neptune-sized moon around the  $\sim 3.2$  Jupiter-mass planet in *Kepler 1625* puts interesting constraints on the formation of the system. In particular, the relatively wide orbit of the moon around the planet, at  $\sim 40$  planetary radii, is hard to reconcile with planet formation theories. We demonstrate that the observed characteristics of the system can be explained from the tidal capture of a secondary planet in the young system. After a quick phase of tidal circularization, the lunar orbit, initially much tighter than 40 planetary radii, subsequently gradually widened due to tidal synchronization of the spin of the planet with the orbit, resulting in a synchronous planet-moon system. Interestingly, in our scenario the captured object was originally a Neptune-like planet, turned into a moon by its capture.

*Key words:* planets and satellites: dynamical evolution and stability – planets and satellites: formation

## 1. Introduction

First-of-its-kind discoveries generally put interesting constraints on our understanding. The first planet (Wolszczan & Frail 1992) as well as the first Solar system-passing interstellar asteroidal-object (Bacci et al. 2017; Meech et al. 2017a, 2017b) surprised many theorists and started a flurry of speculations on their origin. A first moon discovered outside of the Solar system would also pose a number of interesting constraints and possibilities for its origin.

A candidate for such a moon (a natural satellite that orbits an exoplanet) was recently found around the  $\sim 1.079 M_{\odot}$  mass star 2MASS J19414304+3953115 (Mathur et al. 2017). Since the discovery of a  $\sim 3.2 M_J$  planet in a circular  $\sim 0.84$  au orbit, this system has become known as *Kepler 1625*.<sup>3</sup>

Compelling evidence for a Neptune-like moon orbiting the  $\sim 3.2 M_J$  planet *Kepler 1625 b* at a separation of  $\sim 40$  planetary radii was recently found (Teachey et al. 2018; Teachey & Kipping 2018; however, there exists the possibility that the exomoon signal is a false positive; see Rodenbeck et al. 2018). This hypothetical moon, *Kepler 1625b I*, is remarkably massive (with a mass of about 1/100 of the planetary mass) and large compared to *Kepler 1625b*, and poses an intriguing problem regarding its formation. Teachey & Kipping (2018) speculate that its origin challenges theorists (this is emphasized in Heller 2018, who considered a tidal capture scenario, although through planet-binary encounters).

In this Letter, we argue that, although the (hypothetical) moon puts interesting constraints on the early dynamical evolution of the planet-moon system, its existence is not surprising. According to our understanding, the current moon was born a planet in orbit around the star 2MASS J19414304+3953115. This planet turned into a moon upon its tidal capture with the more massive planet. Further tidal interaction circularized and widened the orbit due to angular momentum transfer from the spin of the planet to the orbit until synchronization. For convenience, we will use the term “planet” for the giant planet *Kepler 1625b*, and “moon” for

its companion *Kepler 1625b I*, although both should be referred to as planets according to this scenario.

We demonstrate that this process is feasible, and leads to massive moons in relatively wide ( $\gtrsim 10 R_{\text{planet}}$ ) orbits around relatively old ( $\gtrsim 1$  Gyr) stars. In our scenario, we predict that the planet and moon are currently synchronized with their orbit, and we can put constraints on the primordial spin of the planet.

In Section 2, we consider simple analytic arguments for the conditions of capture, and investigate the primordial spin of the planet necessary to explain the current orbit. We give an explicit numerical example of the secular tidal evolution after capture in Section 3. We discuss the likelihood of our scenario in Section 4, and conclude in Section 5.

## 2. Analytic Estimates

We recognize four distinct stages, which we illustrate in Figure 1.

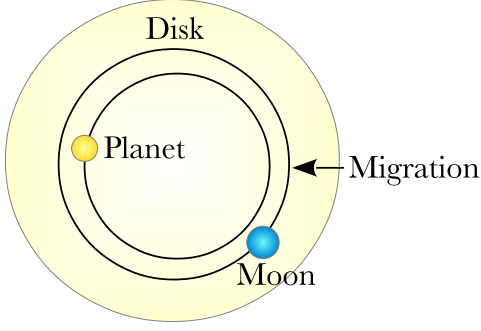
1. Migration and scattering: two planets embedded in a protoplanetary disk migrate toward similar orbits, triggering a short-lived phase of dynamical instability.
2. Capture: during the dynamical instability phase, the lighter planet (henceforth “moon,” with mass and radius  $M_m$  and  $R_m$ , respectively) approaches the more massive planet (with mass and radius  $M_p$  and  $R_p$ , respectively) to a distance  $r_{\text{per}}$ , leading to a strong tidal encounter that initiates its capture.
3. Circularization: the moon is initially captured onto a wide and highly eccentric orbit (but still within the planet’s Hill radius,  $r_H$ ). Tidal dissipation subsequently leads to the circularization of the orbit.
4. Synchronization: residual spin angular momentum of the planet (spin frequency  $\Omega_p$ ) is gradually transferred to the orbit of the moon around the planet, resulting in expansion until synchronization is reached.<sup>4</sup>

We write the moment of inertia of the planet and the moon as  $I_p = r_{g,p} M_p R_p^2$ , and  $I_m = r_{g,m} M_m R_m^2$ , respectively. Here,  $r_{g,p}$  is the gyration radius of the planet, and  $r_{g,m}$  for the moon, and we

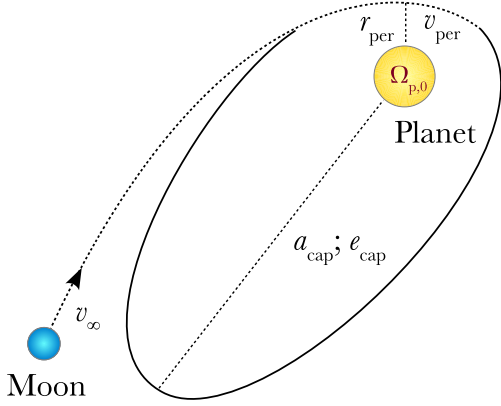
<sup>4</sup> As the moment of inertia of the moon is much smaller than that of the planet (see below), the moon cannot transfer a significant amount of angular momentum, and is quickly synchronized with the orbit.

<sup>3</sup> See <https://exoplanets.nasa.gov/newworldsatlas/2271/kepler-1625b/>.

# 1. Migration & Scattering



## 2. Capture



## 3. Circularization 4. Synchronization

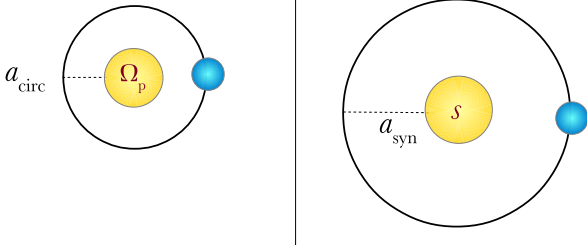


**Figure 1.** Sketch of the scenario of tidal capture. In stage 1, the star is not shown, and only one possibility of convergent migration is shown (the moon outside, and migrating inward). The symbols used are described in the text.

assume that both have a value of 0.25. We adopt the “canonical” values of  $M_p = 10^3 M_\oplus \simeq 3.15 M_J$ ,  $R_p = 11.4 R_\oplus$  for the planet, and  $M_m = 10 M_\oplus \simeq 0.0135 M_J$ ,  $R_m = 4.0 R_\oplus$  for the moon (Teachey & Kipping 2018). For these values,  $I_p/I_m \simeq 812$ , and we can safely neglect the spin angular momentum of the moon. We furthermore define the reduced mass  $\mu \equiv M_p M_m / M$ , where  $M \equiv M_p + M_m$ .

### 2.1. Conditions for Tidal Capture

We assume that the moon approaches the planet on a hyperbolic orbit with periastron distance  $r_{\text{per}}$ . When the interaction results from the gradual migration of the planet or moon, both orbits are similar upon the tidal encounter, and we expect their relative velocity (i.e., the hyperbolic velocity at infinity),  $v_\infty$ , to be small. We set  $v_\infty$  to be a fraction  $\alpha$  of the

circular orbital velocity at the separation of the planet+moon system, i.e.,

$$v_\infty = \alpha \sqrt{GM_\star / a_\star}, \quad (1)$$

where  $M_\star = 1.079 M_\odot$  is the stellar mass, and  $a_\star = 0.84 \text{ au}$  (Mathur et al. 2017).

The initial orbital energy is  $\mu v_\infty^2 / 2$ . For tidal capture to be successful, sufficient energy should be dissipated in the planet and moon during the first passage to produce a bound orbit. In addition, after first passage the apoapsis distance should remain well within the Hill radius,  $r_H$ ; otherwise, the star will perturb the newly captured moon’s orbit, preventing its return to the planet. Approximately, this condition is described by

$$a_{\text{cap}} < r_H / 2, \quad (2)$$

where  $a_{\text{cap}}$  is the semimajor axis of the planet-moon orbit directly after tidal capture. Here,

$$r_H = a_\star \left( \frac{M}{3M_\star} \right)^{1/3}, \quad (3)$$

is the planet’s Hill radius. The factor 2 in Equation (2) takes into account that the captured orbit is initially highly eccentric; therefore,  $r_H$  should be compared to the apoapsis distance  $a_{\text{cap}}(1 + e_{\text{cap}}) \approx 2 a_{\text{cap}}$ .

We calculate  $a_{\text{cap}}$  from the conservation of energy. Specifically, we consider the initial energy and the energy after first passage. The latter consists of the (negative) orbital energy, and the amount of energy dissipated in the tides,  $\Delta E_{\text{tides}}$  ( $\Delta E_{\text{tides}} > 0$ ). Therefore,

$$\frac{1}{2} \mu v_\infty^2 = -\frac{G\mu M}{2a_{\text{cap}}} + \Delta E_{\text{tides}}. \quad (4)$$

We use the formalism of Press & Teukolsky (1977) to compute  $\Delta E_{\text{tides}}$  in both the planet and moon as a function of the masses, radii, and the periastron distance  $r_{\text{per}}$ . Specifically,  $\Delta E_{\text{tides}} = \Delta E_{\text{tides,p}} + \Delta E_{\text{tides,m}}$ , where

$$\Delta E_{\text{tides},i} = \frac{GM_{3-i}^2}{R_i} \sum_{l=2}^3 \left( \frac{R_i}{r_{\text{per}}} \right)^{2l+2} T_l(\eta_i), \quad (5)$$

with

$$\eta_i \equiv \left( \frac{M_i}{M} \right)^{1/2} \left( \frac{r_{\text{per}}}{R_i} \right)^{3/2}. \quad (6)$$

Here,  $M_{3-i}$  is the companion mass. The dimensionless functions  $T_l(\eta_i)$  depend on the structure of the planet/moon. We assume polytropic pressure-density relations, and adopt analytic fits to  $T_l(\eta_i)$  for polytropic indices of  $n = 1.5$  or  $2$  as determined by Portegies Zwart & Meinen (1993). In Equation (5), we take the two lowest-order harmonic modes ( $l = 2$  and  $l = 3$ ), which give a good description (Press & Teukolsky 1977).

The analytic fits for  $T_l(\eta)$  from Portegies Zwart & Meinen (1993) do not account for the planetary and lunar spins. In the case of significant spins, however,  $T_l(\eta)$  could be a few times larger. For simplicity, we ignore this complexity, but note that this adds some uncertainty to our calculation of  $a_{\text{cap}}$ .

In Figure 2, we plot  $a_{\text{cap}}$  as a function of  $r_{\text{per}}$  according to Equation (4). We assume the canonical radii, and consider different combinations of  $v_\infty$  (quantified by  $\alpha$ ), and the polytropic index  $n$  (a larger  $n$  corresponds to a more centrally

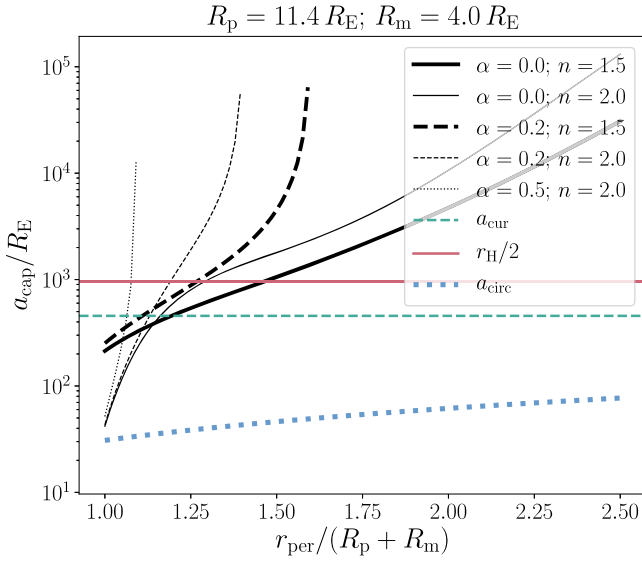


**Figure 2.** Capture semimajor axis  $a_{\text{cap}}$  as a function of the periastron distance  $r_{\text{per}}$  according to Equation (4). The canonical radii are assumed, with different combinations of  $v_{\infty}$  (quantified by  $\alpha$ ) and the polytropic index  $n$ . The red solid (green dashed) horizontal line shows  $r_{\text{H}}/2$  ( $a_{\text{cur}}$ , the current semimajor axis). The blue dotted line shows  $a_{\text{circ}}$  (see Equation (7)).

concentrated planet/moon). A polytropic index of  $n = 1.5$  is a reasonable approximation for the structure of a gas giant planet (Weppner et al. 2015). The red solid (green dashed) horizontal line shows  $r_{\text{H}}/2$  ( $a_{\text{cur}}$ , the current semimajor axis, which we set to  $a_{\text{cur}} = 40 R_{\text{p}} = 456 R_{\oplus}$ ). With our parameters, tidal energy dissipation during the capture is dominated by the moon, with  $\Delta E_{\text{tides,m}}/\Delta E_{\text{tides}} \simeq 0.94$  for  $r_{\text{per}}/(R_{\text{p}} + R_{\text{m}}) = 1$ , and increasing to  $\Delta E_{\text{tides,m}}/\Delta E_{\text{tides}} \simeq 0.98$  for  $r_{\text{per}}/(R_{\text{p}} + R_{\text{m}}) = 1.5$ .

For sufficiently small  $r_{\text{per}}$ , the moon can be tidally captured without its orbit being perturbed by the star. The range in  $r_{\text{per}}$  is typically small, but increases for smaller  $v_{\infty}$  (i.e., smaller  $\alpha$ ) and smaller  $n$ . The range of  $r_{\text{per}}$  increases for a smaller planet. This is shown explicitly in Figure 3, in which the largest periastron distance for which capture is possible,  $r_{\text{per,max}}$ , is plotted as a function of  $R_{\text{p}}$ , for different combinations of  $R_{\text{m}}$ ,  $\alpha$ , and  $n$ .

## 2.2. Orbital Expansion Due to Secular Tidal Evolution

After tidal capture, the orbit is highly eccentric. Subsequently, the orbit shrinks and circularizes. The semimajor axis after circularization can be estimated as

$$a_{\text{circ}} \simeq 2 r_{\text{per}}. \quad (7)$$

Tidal capture alone cannot explain the current orbit of the planet-moon system in *Kepler 1625*. This is exemplified in Figure 2, in which  $a_{\text{circ}}$  is shown with the blue dotted curves. For any reasonable values of  $r_{\text{per}}$ ,  $a_{\text{circ}}$  is smaller than the currently observed semimajor axis,  $a_{\text{cur}}$ , by about an order of magnitude. Here, we set  $a_{\text{cur}}$  to  $40 R_{\text{p}} = 456 R_{\oplus}$ .

After capture, the expansion of the orbit to the currently observed orbit is mediated by the transfer of angular momentum from the spin of the planet to the orbit. This process continues until the planet and orbit are in synchronous rotation (analogous to the current tidal evolution of the Earth-Moon system).

Using the fact that angular momentum is conserved during the entire process (capture, circularization, and synchronization), we can equate the initial angular momentum before

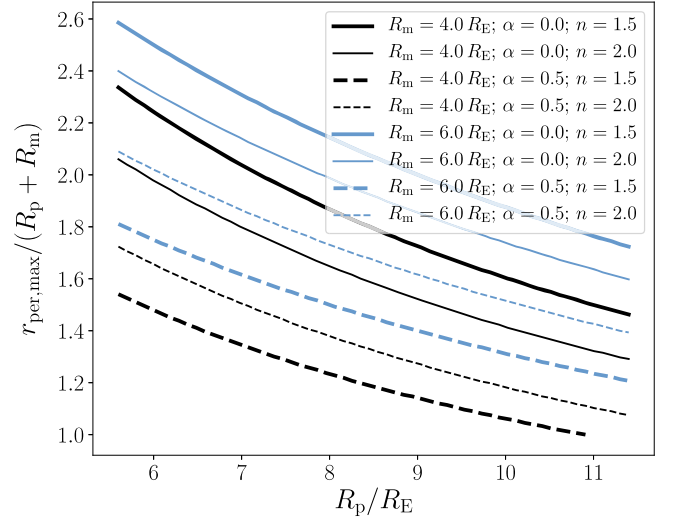


**Figure 3.** Largest periastron distance for which capture is possible,  $r_{\text{per,max}}$ , plotted as a function of  $R_{\text{p}}$ , and for different combinations of  $R_{\text{m}}$ ,  $\alpha$ , and  $n$ .

capture to the angular momentum after synchronization. After synchronization, the planetary spin frequency is equal to the orbital frequency,  $s = \sqrt{GM/a_{\text{syn}}^3}$ , where  $a_{\text{syn}}$  is the semimajor axis of the synchronized orbit. Therefore, neglecting the moon's spin angular momentum,

$$\mu v_{\text{per}} r_{\text{per}} + I_{\text{p}} \Omega_{\text{p},0} = \mu \sqrt{GM a_{\text{syn}}} + I_{\text{p}} \sqrt{\frac{GM}{a_{\text{syn}}^3}}. \quad (8)$$

Here,  $\Omega_{\text{p},0}$  is the spin frequency of the planet before the tidal encounter (i.e., the primordial spin frequency), and  $v_{\text{per}}$  is the orbital speed at periastron at first approach. We compute  $v_{\text{per}}$  by assuming a purely hyperbolic orbit on first approach, i.e.,

$$v_{\text{per}} = \sqrt{v_{\infty}^2 + \frac{2GM}{r_{\text{per}}}}. \quad (9)$$

Writing the initial planet's spin as  $\Omega_{\text{p},0} = \beta \sqrt{GM_{\text{p}}/R_{\text{p}}^3}$ , where  $\beta$  is a dimensionless parameter that measures the initial planetary spin in units of its breakup rotation rate, we obtain from Equations (1), (8), and (9) the following expression for the minimum required spin of the planet such that the synchronized orbit has semimajor axis  $a_{\text{syn}}$ ,

$$\beta = \sqrt{\frac{M}{M_{\text{p}}}} \left[ \left( \frac{R_{\text{p}}}{a_{\text{syn}}} \right)^{3/2} + \frac{M_{\text{m}}}{M} r_{\text{g,p}}^{-1} \left( \sqrt{\frac{a_{\text{syn}}}{R_{\text{p}}}} - \sqrt{\frac{2r_{\text{per}}}{R_{\text{p}}}} \sqrt{1 + \alpha^2 \frac{M_{\star}}{M} \frac{r_{\text{per}}}{2a_{\star}}} \right) \right]. \quad (10)$$

After circularization, the orbit asymptotically evolves to synchronization, expanding the orbit in the process. The associated timescale depends on the efficiency of tidal dissipation (see Section 3 below). We expect the currently observed orbit to be close to synchronization. Therefore, by setting  $a_{\text{syn}} = a_{\text{cur}}$ , we can use Equation (10) to determine, as a function of  $r_{\text{per}}$ , the minimal initial planetary spin (quantified by  $\beta$ ) required to explain the currently observed orbit.

In Figure 4, we present the resulting values for  $\beta$  for a selection of values for  $\alpha$  and  $n$ . The vertical lines (in red)

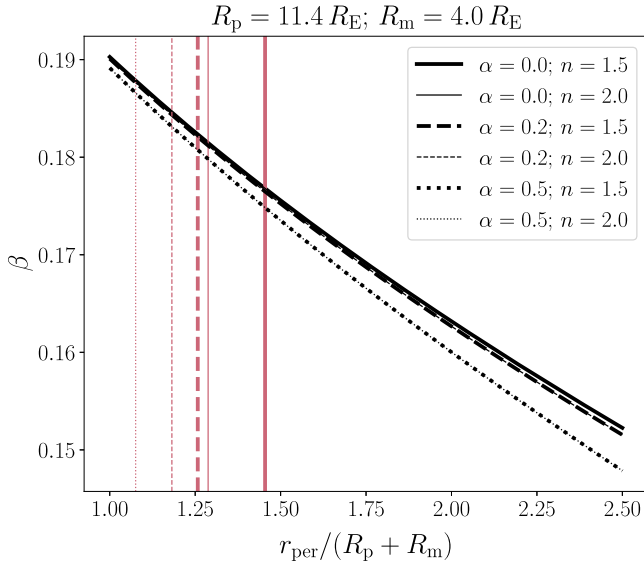


**Figure 4.** Initial planetary spin (quantified by the fraction  $\beta$  of breakup rotation) required to explain the current orbit of *Kepler* 1625 through tidal capture, as a function of  $r_{\text{per}}$ . Assumed radii are  $R_p = 11.4 R_{\oplus}$  and  $R_m = 4 R_{\oplus}$ . Different line styles and thicknesses correspond to different  $\alpha$  and  $n$ . The vertical red lines indicate the maximum  $r_{\text{per}}$  for which capture can be successful.

indicate the maximum value of  $r_{\text{per}}$  below which capture can be successful, i.e.,  $a_{\text{cap}} < r_{\text{H}}/2$ , assuming  $R_p = 11.4 R_{\oplus}$  and  $R_m = 4 R_{\oplus}$ . The dependence of  $\beta$  on  $r_{\text{per}}$  is not strong; generally,  $\beta \sim 0.2$ , i.e., 20% of breakup rotation is required. For  $R_p = 5.6 R_{\oplus}$  and  $R_m = 4 R_{\oplus}$  (not shown here), the allowed (normalized) range in  $r_{\text{per}}/(R_p + R_m)$  is larger, but the required  $\beta$  to explain the current orbit is larger; typically,  $\beta \sim 0.3$ . The minimum value for  $\beta$  is lower for non-zero  $\alpha$  (in which case some angular momentum can be transferred from the initial orbit to the planetary spin), but the differences between  $\alpha = 0$  and  $\alpha = 0.5$  are small.

A rotation rate of a few tens of percent of breakup rotation is not extreme nor unusual. For example, Jupiter, Saturn, and Neptune are rotating at  $\simeq 0.3$ , 0.4, and 0.2 of breakup rotation, respectively. Massive Jupiter-like extrasolar planets are known to have similar rotation rates (see, e.g., Figure 2 of Bryan et al. 2018).

### 3. Numerical Example of Secular Tidal Evolution

In Section 2, we derived analytic expressions for the tidal evolution of the planet-moon system after capture. Here, we illustrate the long-term tidal evolution that results from the capture of the moon by the planet by integrating the secular equations of motion numerically.

We adopt the equilibrium tide model by Eggleton et al. (1998), with the apsidal motion constants  $k_{\text{AM,p}} = k_{\text{AM,m}} = 0.19$ . For the tidal time-lags, we adopt either  $\tau = \tau_p = \tau_m = 6.6$  s or 66 s. A value of  $\tau = 6.6$  s corresponds to 10 times longer (i.e., stronger tides) than 0.6 s, as inferred to be appropriate for high-eccentricity migration by Socrates et al. (2012). These efficient tides turn out to be necessary to explain the current orbit with our nominal parameter values (see below). For simplicity, we use the equilibrium tide model for the evolution immediately after capture, when the eccentricity is still high ( $e > 0.9$ ). A caveat of

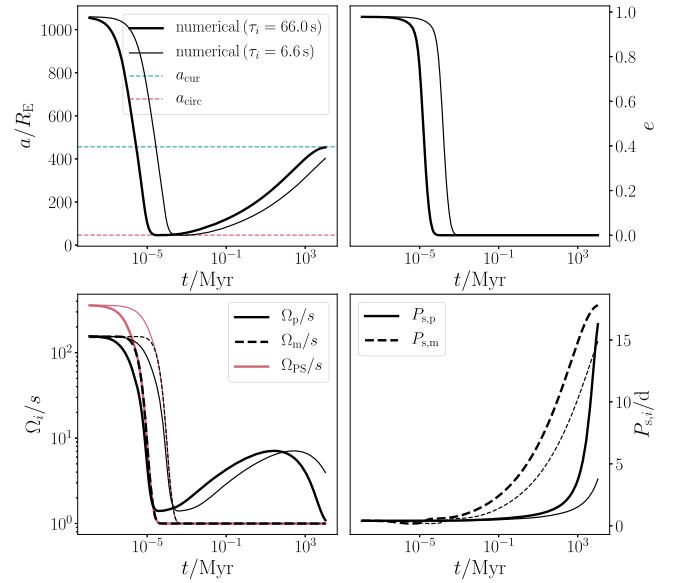


**Figure 5.** Long-term evolution of the semimajor axis (top-left panel), eccentricity (top-right panel), the spin rates normalized to the orbital mean motion  $s$  (bottom-left panel), and the rotation periods (bottom-right panel) in a tidal capture scenario for *Kepler* 1625, obtained by numerically integrating the secular tidal equations of motion. Thick and thin lines correspond to a time lag of 66 and 6.6 s, respectively. In the top-left panel, the green dashed line indicates the current semimajor axis of the planet-moon orbit; the red dashed line shows the expected circularization semimajor axis, Equation (7). In the bottom-left panel, the red lines show the expected curves for pseudosynchronous rotation computed using Equation (42) of Hut (1981) and the eccentricity as a function of time from the numerical simulations.

this is that the equilibrium tide model does not accurately describe the evolution for eccentricities  $\gtrsim 0.8$  (Mardling 1995).

We start the integration with a semimajor axis of  $a_0 \simeq 1060 R_{\oplus}$ . This value corresponds to (borderline) capture at  $r_{\text{per}} = 1.5(R_p + R_m)$  with  $\alpha = 0$  and  $n = 1.5$  (see Figure 2). The corresponding initial eccentricity is  $e_0 = 1 - r_{\text{per}}/a_0 \simeq 0.978$ . According to our analytic estimates (see Figure 4), the critical planetary spin for the final orbit to match the current orbit is  $\beta \simeq 0.1756$ . We adopt this spin rate for the planet. The rotation period of the moon is set to 10 hr; note, however, that the latter does not affect the synchronized semimajor axis because  $I_p \gg I_m$ . In the numerical integrations, the spins are assumed to be initially aligned with the orbit.

We present in Figure 5, the time evolution of the semimajor axis, eccentricity, and the spin rates, where the integration lasts for 10 Gyr, approximately the age of the star (Teachey & Kipping 2018). The thick and thin lines correspond to a time lag of 66 and 6.6 s, respectively. The initial evolution is rapid, circularizing and shrinking the orbit to a value that is consistent with  $a_{\text{circ}}$  (red dashed line in the top-left panel; see Equation (7)) within  $\sim 10$  yr. The moon, which has a small moment of inertia, is synchronized within the same time span, whereas the planet remains spinning more rapidly than the orbit for up to  $\sim 10$  Gyr. The planet is synchronized within  $\sim 10$  Gyr assuming extremely efficient tides ( $\tau = 66$  s), and the steady-state semimajor axis is consistent with the currently observed value (green dashed line; this is consistent with the analytic expression for  $\beta$  presented in Equation (10)). Assuming less efficient tides ( $\tau = 6.6$  s), equilibrium is not yet reached after 10 Gyr, although it is close ( $a$  reaching  $a_{\text{cur}}$  within  $\simeq 13\%$ ). Evidently, even weaker tides would make the agreement with the current orbit within 10 Gyr more difficult.

We can estimate the timescales for circularization and synchronization analytically as follows. Circularization is dominated by the tides in the moon, and during the circularization phase, the spins are quickly brought to pseudosynchronous rotation (see Equation (42) of Hut 1981, and the red lines showing  $\Omega_{\text{ps}}/s$  in the bottom-left panel of Figure 5). Also taking the limit  $e \rightarrow 1$ , the circularization timescale can then be estimated as (Hut 1981)

$$t_e \equiv \left( \frac{1}{e} \frac{de}{dt} \right)^{-1} \\ \sim (1 - e^2)^{13/2} \left( \frac{a_0}{R_m} \right)^8 \frac{T_m}{k_{\text{AM},m}} \frac{1}{q_m(1 + q_m)} \frac{1}{27} \frac{320}{451} \\ \simeq 9 \times 10^2 \text{ yr.} \quad (11)$$

Here,  $T_i \equiv R_i^3 / (GM_i \tau_i)$  (Hut 1981, Equation (12)), and  $q_i = M_{3-i} / M_i$ . In the last line of Equation (11), we substituted numerical values, assuming  $\tau_i = 66$  s. The resulting timescale is roughly consistent with the circularization timescale in the numerical example.

To estimate the synchronization timescale, we take advantage of the separation of timescales for circularization and synchronization. After circularization,  $e = 0$  and  $a = a_{\text{circ}} \simeq 2 r_{\text{per}} = 46.2 R_{\oplus}$ , whereas the planetary spin (which dominates the spin angular momentum budget) is still equal to its initial value to good approximation (see the bottom-right panel of Figure 5). In this case, one can show using Equations (9) and (11) of Hut (1981) that  $a$  and  $\Omega_p$  are related according to

$$a^{1/2} - a_{\text{circ}}^{1/2} = -C(\Omega_p - \Omega_{p,0}), \quad (12)$$

where  $C \equiv (1 + q_p) r_{\text{g},p} R_p^2 / (q_p \sqrt{GM})$ . By integrating the equation for  $da/dt$  over time, we find a synchronization timescale

$$t_{\Omega} \equiv \int_{a_{\text{circ}}}^{a_f} \frac{da}{\dot{a}} = \frac{1}{6} \frac{T_p}{k_{\text{AM},p}} \left( \frac{a_{\text{circ}}}{R_p} \right)^8 \frac{1}{q_p(1 + q_p)} \\ \times \int_1^{a_f/a_{\text{circ}}} \frac{x^7 dx}{x^{3/2} [A - B(x^{1/2} - 1)] - 1} \\ \simeq 2 \times 10^{10} \text{ yr.} \quad (13)$$

Here,  $A \equiv \Omega_{p,0} \sqrt{a_{\text{circ}}^3 / (GM)}$ ,  $B \equiv a_{\text{circ}}^2 / (C \sqrt{GM})$ , and  $a_f$  is the final semimajor axis. For the numerical estimate, we again assumed  $\tau_i = 66$  s, whereas we set  $a_f = 0.99 a_{\text{cur}}$ . The numerical value is roughly consistent with the synchronization timescale in Figure 5.

#### 4. Discussion

Multiple bodies form during the early evolution of a debris disk to a fully populated planetary system. The migration of planets in such an environment is to be expected, in particular when the residual gas causes a drag force on the planets. The efficiency of this drag force is proportional to the planet mass (Dürmann & Kley 2015). For a tidal capture to become possible, the two planets have to acquire similar orbits, which can be realized via drag. It remains unclear if the more massive planet was born further out and migrated inward to the lower-mass planet, or that the more massive planet originally orbited closer to the star. In the latter case, the disk must have had an

inner edge to prevent the inner more massive planet to migrate further inward.

In both cases, the encounter is expected to occur with comparable orbits; i.e., the encounter is parabolic, or hyperbolic with a relatively low speed at infinity. The outcome of this encounter can be the ejection of one of the planets (most likely the lower-mass planet), collisions with the star, tidal capture, or a collision of the planets with each other. We can estimate the branching ratios between these scenarios by comparing the relevant cross-sections. Here, we do not consider collisions with the star.

For ejections to occur, we require the velocity change imparted on the lower-mass planet (mass  $M_m$ ) during the encounter at a distance of  $\sim a_*$  to be comparable to the local escape velocity from the star, i.e.,  $\Delta v_m \sim v_{\text{esc}} = \sqrt{2GM_*/a_*}$ . The (3D) velocity change for an encounter with impact parameter  $b$  can be estimated as (e.g., Binney & Tremaine 2008, S3.1(d))

$$\Delta v_m \approx \frac{2M_p}{M} \frac{v_{\infty}}{\sqrt{1 + (b/b_{90})^2}}, \quad (14)$$

where  $b_{90} \equiv GM/v_{\infty}^2 = (a_*/\alpha^2)(M/M_*) \simeq (55.4/\alpha^2) R_{\oplus}$  is the impact parameter for a  $90^\circ$  deflection. For  $\alpha \sim 1$ ,  $b_{90} > R_p + R_m$ , showing that gravitational focusing is important. The impact parameter for escape can therefore be written as

$$b_{\text{ej}} = b_{90} \sqrt{2\alpha^2 (M_p/M)^2 - 1}. \quad (15)$$

Note that  $v_{\infty}$  needs to be large enough for the lower-mass planet to be ejected; specifically,  $\alpha \geq \sqrt{(1/2)(M/M_p)} \simeq 0.71$ .

The impact parameter for tidal capture or direct collision, taking into account gravitational focusing, is

$$b = \sqrt{r^2 + \frac{2GM_r}{v_{\infty}^2}} = r \sqrt{1 + 2 \frac{b_{90}}{r}}, \quad (16)$$

where we set  $r = \gamma (R_p + R_m)$  for tidal capture, and  $r = R_p + R_m$  for direct collision. From our analytical estimates (Section 2),  $\gamma \lesssim 2.5$  for a successful capture, depending on the parameters (see Figure 3).

Therefore, the branching ratio between capture and ejection is

$$\frac{b_{\text{cap}}^2}{b_{\text{ej}}^2} = \gamma^2 \frac{(R_p + R_m)^2}{b_{90}^2} \frac{1 + 2 \frac{b_{90}}{\gamma(R_p + R_m)}}{2\alpha^2 (M_p/M)^2 - 1} \\ \approx \frac{2\gamma}{2\alpha^2 (M_p/M)^2 - 1} \frac{R_p + R_m}{b_{90}} \\ = \frac{2\gamma\alpha^2}{2\alpha^2 (M_p/M)^2 - 1} \frac{M_*}{M} \frac{R_p + R_m}{a_*} \\ \simeq \frac{0.56 \gamma\alpha^2}{2\alpha^2 (M_p/M)^2 - 1}, \quad (17)$$

where in the second line we used that  $b_{90} > R_p + R_m$ , and in the fourth line we substituted our adopted values for the masses, the radii, and  $a_*$ . For  $\alpha = 1$  and  $\gamma = 2.5$ , the first line of Equation (17) gives  $b_{\text{cap}}^2/b_{\text{ej}}^2 \simeq 1.9$ ; for  $\alpha = 0.8$  and  $\gamma = 2.5$ , we get  $b_{\text{cap}}^2/b_{\text{ej}}^2 \simeq 4.3$ .

The branching ratio between capture and collision is

$$\frac{b_{\text{cap}}^2}{b_{\text{col}}^2} = \gamma^2 \frac{1 + 2 \frac{b_{90}}{\gamma R_p + R_m}}{1 + 2 \frac{b_{90}}{R_p + R_m}} \approx \gamma, \quad (18)$$

where we again used that  $b_{90} > R_p + R_m$ . For  $\alpha = 1$  and  $\gamma = 2.5$ , the non-approximated Equation (18) gives  $b_{\text{cap}}^2/b_{\text{col}}^2 \simeq 3.0$  (for  $\alpha = 0.8$  and  $\gamma = 2.5$ ,  $b_{\text{cap}}^2/b_{\text{col}}^2 \simeq 2.8$ ). We note that our distinction here between capture and collision is simplistic; e.g., using hydrodynamic simulations, Hwang et al. (2018) showed that interactions with  $r_{\text{per}}/(R_p + R_m) < 1$  can lead to bound pairs of planets/moons, in addition to mergers.

We conclude that the likelihoods for ejection, capture, and collision are comparable within a factor of a few. This is consistent with the more detailed calculations of Podsiadlowski et al. (2010) and Ochiai et al. (2014), who carried out numerical scattering experiments and found roughly equal ejection and capture fractions. The distribution of the relative inclination of captured planets binary is flat (see Ochiai et al. 2014), making the currently observed  $\sim 45^\circ$  angle of the planet-moon orbit with respect to the ecliptic not unlikely.

We note that we assumed constant sizes and static interior structure of the planet and moon. If these properties were allowed to vary due to planetary evolution, the synchronization process could occur differently. In particular, the semimajor axis could stall (Alvarado-Montes et al. 2017), which would reduce the likelihood that planet-spin-boosted tidal capture can explain the current orbit of *Kepler* 1625b I.

Another caveat is that during the migration-induced dynamical instability phase, there could be multiple encounters before a successful capture. During each of these encounters, the system could be disrupted, thereby lowering the capture probability. More detailed  $N$ -body integrations to take this into account are left for future work.

## 5. Conclusions

We argued that the planet-moon system in *Kepler* 1625 is the result of the tidal capture of a secondary planet by the primary planet around the star. As a result of scattering induced by convergent migration in a disk, the two planets approached each other on a low-energy hyperbolic or parabolic orbit, and passed each other within  $\lesssim 2.5(R_p + R_m)$ . The tidal dissipation induced in this encounter subsequently led to the capture of the minor planet by the primary planet, turning the former into a moon. The first tidal encounter led to a highly eccentric and wide orbit, and for capture to be successful, the apocenter should have remained within the planet's Hill sphere. The orbit then circularized to a tight orbit, in  $\sim 10$  yr. Over a much longer timescale of  $\sim 10$  Gyr, the primary planet subsequently transferred its spin angular momentum to the orbit, widening the latter until synchronization. We find that the primary planet must have had a primordial spin of at least  $\sim 20\%$  of critical rotation in order to deposit sufficient angular momentum into the planet-moon orbit to be consistent with the current orbit.

We expect that the current orbit evolves very slowly, and that both the planet and moon are in almost synchronous rotation with the orbit.

These captures are probably not uncommon, being roughly as common as planet collisions. However, the precise frequency for this process to operate remains unclear. We expect that moon formation from tidal capture is not uncommon (see also Podsiadlowski et al. 2010; Ochiai et al. 2014), and probably comparable to the number of planet collisions or ejections.

The capture must have occurred early in the planetary system's evolution (more than a Gyr ago) to allow tidal dissipation to synchronize the system to its current orbit. Our scenario can be tested by measuring the spins of both planet and moon, which should be synchronous with the orbit, and along the same axis as the orbital angular momentum of the planet-moon system.

We thank Jaime Alvarado-Montes, René Heller, David Kipping, and Jean Schneider for comments and discussions, and the anonymous referee for a very helpful report. A.S.H. gratefully acknowledges support from the Institute for Advanced Study, and the Martin A. and Helen Chooljian Membership. S.P.Z. thanks Norm Murray and CITA for the hospitality during his long-term visit.

## ORCID iDs

Adrian S. Hamers  <https://orcid.org/0000-0003-1004-5635>

## References

- Alvarado-Montes, J. A., Zuluaga, J. I., & Sucerquia, M. 2017, *MNRAS*, **471**, 3019
- Bacci, P., Mastripieri, M., Tesi, L., et al. 2017, MPEC, 2017-U181
- Binney, J., & Tremaine, S. 2008, *Galactic Dynamics* (2nd ed.; Princeton, NJ: Princeton Univ. Press)
- Bryan, M. L., Benneke, B., Knutson, H. A., Batygin, K., & Bowler, B. P. 2018, *NatAs*, **2**, 138
- Dürmann, C., & Kley, W. 2015, *A&A*, **574**, A52
- Eggleton, P. P., Kiseleva, L. G., & Hut, P. 1998, *ApJ*, **499**, 853
- Heller, R. 2018, *A&A*, **610**, A39
- Hut, P. 1981, *A&A*, **99**, 126
- Hwang, J., Chatterjee, S., Lombardi, J., Jr., Steffen, J. H., & Rasio, F. 2018, *ApJ*, **852**, 41
- Mardling, R. A. 1995, *ApJ*, **450**, 732
- Mathur, S., Huber, D., Batalha, N. M., et al. 2017, *ApJS*, **229**, 30
- Meech, K. J., Bacci, P., Mastripieri, M., et al. 2017a, MPEC, 2017-U183
- Meech, K. J., Kley, J., Wells, L., et al. 2017b, MPEC, 2017-W52
- Ochiai, H., Nagasawa, M., & Ida, S. 2014, *ApJ*, **790**, 92
- Podsiadlowski, P., Rappaport, S., Fregeau, J. M., & Mardling, R. A. 2010, *ApJ*, submitted (arXiv:1007.1418)
- Portegies Zwart, S. F., & Meinen, A. T. 1993, *A&A*, **280**, 174
- Press, W. H., & Teukolsky, S. A. 1977, *ApJ*, **213**, 183
- Rodenbeck, K., Heller, R., Hippke, M., & Gizon, L. 2018, *A&A*, **617**, A49
- Socrates, A., Katz, B., & Dong, S. 2012, arXiv:1209.5724
- Teachey, A., & Kipping, D. M. 2018, *SciA*, **4**, 1784
- Teachey, A., Kipping, D. M., & Schmitt, A. R. 2018, *AJ*, **155**, 36
- Weppner, S. P., McKelvey, J. P., Thielen, K. D., & Zielinski, A. K. 2015, *MNRAS*, **452**, 1375
- Wolszczan, A., & Frail, D. A. 1992, *Natur*, **355**, 145